Drug Delivery

Deutsche Ausgabe: DOI: 10.1002/ange.201509182
Internationale Ausgabe: DOI: 10.1002/anie.201509182

A Telomerase-Specific Doxorubicin-Releasing Molecular Beacon for Cancer Theranostics

Yi Ma, Zhaohui Wang, Min Zhang, Zhihao Han, Dan Chen, Qiuyun Zhu, Weidong Gao, Zhiyu Qian, and Yueqing Gu**

Abstract: *A molecular beacon-based drug delivery system was designed for both detection of telomerase activity in living cells and telomerase-triggered drug release for precise cancer treatment. This system is composed of a gold nanoparticle core densely packed with FITC-labeled hairpin DNA sequences hybridized with telomerase primers. Molecules of the anticancer drug doxorubicin were intercalated into the stem region of the DNA sequence. The presence of telomerase will elongate the primers, leading to inner chain substitution followed by the release of the FITC fluorescence and the trapped doxorubicin. This molecular beacon could specifically distinguish tumor cells and normal cells based on telomerase activity, precisely release doxorubicin in response to telomerase activity in the tumor cells, and prevent toxicity to normal organs.*

Human telomerase is a unique ribonucleoprotein that can increase the number of telomeric repeats to the ends of telomeres to maintain continuous cell proliferation.[1] Telomerase is expressed in 85–90% of human cancer cells, and plays a role in limitless cancer cell division by preventing telomeric shortening. In contrast, telomerase is almost absent in normal cells.[2] This distinct difference in telomerase activity between normal and cancerous cells could serve as a biological principle for the design of telomerase-responsive drug carriers, which may facilitate more precise and easily controlled drug release than the conventional methods of stimuli-responsive drug delivery systems (DDS).[3] In addition, telomerase activity may be an indicator of increased cancer progression.[4] Thus, the detection of telomerase is also of great importance for cancer diagnosis, prognosis, and response to therapy.

Herein, we report a telomerase-responsive gold nanoparticle-based molecular beacon (Dox-AuNP-MB) for both the visualization of intracellular telomerase activity in living cells, as well as the precise drug delivery to cancer cells (Figure 1). The Dox-AuNP-MBs are composed of a gold nanoparticle (AuNP) core that is densely packed with unique hairpin DNA sequences (Seq-1) linked by Au–S bonds at 3′ end of the sequence. The base sequence of the 3′ terminal region is designed to hybridize with telomerase primers (TP). The 5′ terminal region labeled with FITC contains the same sequence as the telomeric repeats, and hybridizes with the inner chain to form the stem part of the hairpin sequence. The FITC fluorescence from the 5′ label is quenched as a result of the proximity to the gold nanoparticles.[5] Doxorubicin (Dox) molecules are then inserted into the GC base pairs of the stem part. In the presence of telomerase, the primer is elongated to produce telomeric repeats that competitively hybridize with the stem part of the hairpin sequence, resulting in the substitution of 5′ region of the sequence and subsequent opening of the loop. This substitution process triggers the release of the quenched FITC and trapped Dox for accurate diagnosis and precise drug delivery in tumor cells. Thiol polyethylene glycol (SH-PEG) modification is used to enhance the stability and reduce the immunogenicity of Dox-AuNP-MBs.[6]

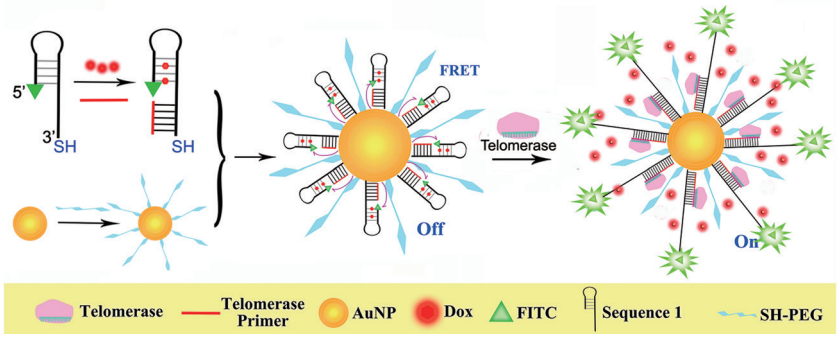

Figure 1. Illustration of the synthesis of Dox-AuNP-MBs and telomerase-triggered fluorescence recovery and drug release.

First, the gold nanoparticle-based molecular beacon (AuNP-MB) for telomerase detection was successfully prepared and characterized (Supporting Information, Figure S1). The average diameter of AuNP-MBs was approximately 15 nm (Figure S1 b), which was similar to that of the AuNPs (Figure S1 a) but with higher dispersibility owing to PEG

[*] Y. Ma, Z. Wang, M. Zhang, Z. Han, D. Chen, Q. Zhu, W. Gao, Prof. Dr. Y. Gu
State Key Laboratory of Natural Medicines
Department of Biomedical Engineering
School of Engineering, China Pharmaceutical University
24 Tongjia Road, Nanjing, 210009 (China)
E-mail: guyueqingsubmission@hotmail.com
Prof. Dr. Z. Qian
Department of Biomedical Engineering
School of Automation
Nanjing University of Aeronautics and Astronautics
29 Yudao Street, Nanjing, 210016 (China)

Supporting information and ORCID(s) from the author(s) for this article are available on the WWW under http://dx.doi.org/10.1002/anie.201509182.

modification. PEG is an electrically neutral ligand that can effectively prevent the aggregation of gold nanoparticles. Dynamic light scattering data showed that the hydrodynamic diameters of AuNPs and AuNP-MBs were 43.3 nm and 51.6 nm, respectively, indicating that the surface coating increased the diameter of MB (Figure S1 a, S1 b). Compared to AuNPs with an absorption peak only at 520 nm, the UV/Vis spectrum of AuNP-MBs also showed a characteristic DNA peak at 260 nm (Figure S1 c), confirming the successful conjugation of DNA sequences to the gold surface. As shown in Figure S1 d, the initial solution of AuNP-MBs exhibited no fluorescent signal, suggesting that the FITC fluorescence was efficiently quenched by the AuNPs. After the addition of telomerase and dNTPs, a significant increase in fluorescent intensity was observed, verifying the telomerase-triggered fluorescence switch.

To investigate the stability of AuNP-MBs against damage by intracellular enzymes and reductants, DNase I, T4 DNA ligase, and GSH were individually added to AuNP-MBs, and almost no fluorescent signal was observed. In contrast, the addition of telomerase or the strong reductant DTT led to a substantial increase in fluorescence (Figure S1 e). Gel electrophoresis confirmed that the fluorescence recovery by DTT treatment resulted from the break of the Au–S bond and detachment of DNA from AuNP, and the fluorescence signal after telomerase treatment was attributed to primer extension and substitutional hybridization. The results also indicated that the DNA sequences coated on the gold nanoparticle surface were not degraded by DNase I (Figure S2). The stability of AuNP-MBs was also confirmed in different media, such as PBS, DMEM with 10% FBS, and whole blood (Figure S1 f). Collectively, these results verified the telomerase-specificity and structural stability of AuNP-MBs, and provided the basis for cellular and in vivo applications.[7]

The cellular uptake of AuNP-MBs was monitored on human malignant glioma (U87) cells by hyperspectral microscopy (Figure S3 a). The increase of the reflection signal within the first 90 minutes displayed the gradual accumulation of AuNP-MBs in the cytoplasm, as nanoparticles of 15 nm diameter could not penetrate the nucleopore. The intracellular tracking of the telomerase activity was evaluated by the recovered FITC fluorescence from AuNP-MBs under confocal laser scanning microscopy (CLSM). As shown in Figure S3 b, FITC fluorescence intensity gradually increased in the cytoplasm as the incubation time increased, which displayed a similar time profile to the cellular uptake of AuNP-MBs (Figure S3 a). FITC fluorescence images at different depths along the z-axis of cancer cells was also obtained (Figure S3 c). Importantly, these images revealed the efficient cellular uptake and sensitive response of the AuNP-MBs, which is a prerequisite for telomerase detection and drug delivery in the subsequent experiments. In addition, the impact of the ratio between the DNA sequence and AuNPs on diagnostic efficacy was investigated (Figure S4). The strongest fluorescence signal was found in the 80:1 group because of the abundance of DNA-loading and appropriate steric hindrance.

To confirm that the fluorescence in tumor cells was indeed triggered by telomerase, U87 cells with different levels of telomerase were obtained by pre-treating with different concentrations of epigallocatechin gallate (EGCG), a well-characterized telomerase inhibitor. As shown in Figure 2 a, the fluorescence intensity gradually reduced with increasing amounts of EGCG (Figure 2 b), confirming that AuNP-MBs

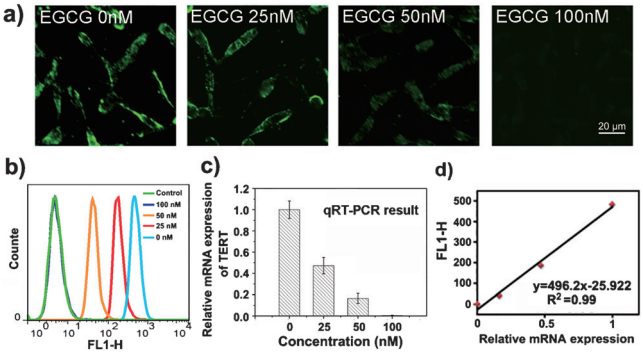

Figure 2. a) CLSM images of U87 cells after incubation with different concentrations of EGCG (0, 25, 50, and 100 nM) for 48 hours, then incubated with 0.2 mL AuNP-MBs (6 nM) for 1.5 h. Scale bar = 20 μm. b) Flow cytometric detection of U87 cells after treatment with EGCG (0, 25, 50, and 100 nM) for 48 hours, then incubated with 0.2 mL AuNP-MBs (6 nM) for 1.5 h. c) Relative TERT mRNA expression of U87 cells treated with EGCG (0, 25, 50, and 100 nM). d) Linear fitting between the relative TERT mRNA expression by qRT-PCR and fluorescence intensity of AuNP-MBs by flow cytometry.

were specific to telomerase activity. Because the expression of TERT can reflect telomerase activity, qRT-PCR assays were performed to examine TERT expression in these four groups of pre-treated cells (Figure 2 c). Linear fitting was performed between the relative TERT mRNA expression levels and FITC-fluorescence intensity with linearity up to 0.99, indicating excellent reliability and accuracy of the detection using AuNP-MBs (Figure 2 d). Therefore, by precisely reflecting telomerase activity with corresponding fluorescence intensity, the AuNP-MBs could be used for quantitative analysis of intracellular telomerase activity.

Based on the results above, we further used this AuNP-MB to track the telomerase activity in four different cell lines, including U87 (human malignant glioma cells), MCF-7 (human breast cancer cells), L02 (human hepatocytes), and HEK293 (human embryonic kidney cells). Confocal images revealed that U87 cells showed higher telomerase activity than MCF-7 cells, but no telomerase activity was found in the noncancerous cell lines, L02 and HEK293 (Figure S5 a). The distinctive fluorescence intensities of cancerous and normal cells were consistent with TERT gene expression using qRT-PCR (Figure S5 b). These results suggested that our AuNP-MBs could be used for quick and accurate identification of cancer cells, which has promising potential for clinical cancer diagnostics.

For AuNP-MBs to be an effective probe, it must be applicable in mixed populations of both cancer and normal cells. Co-cultured U87 and L02 cells were incubated with AuNP-MBs for 1.5 hours. As shown in Figure 3 a, fluorescence was only observed in the cytoplasm of U87 cells, however no fluorescent signal was found in L02 cells,

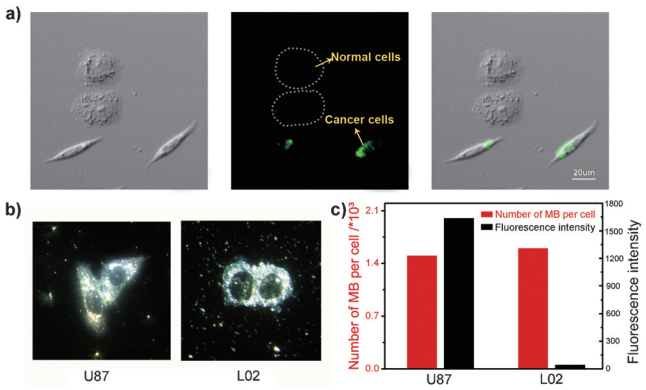

Figure 3. a) CLSM images of co-cultivation of U87 cells (cancer cells) and L02 cells (normal cells) in one confocal dish after incubation with 0.2 mL AuNP-MBs (6 nM) for 1.5 h. Scale bar = 20 μm. b) Hyperspectral microscopy imaging of U87 and L02 cells after incubation with 0.2 mL AuNP-MBs (6 nM) for 1.5 h. c) ICP-AES for quantifying the amount of AuNP-MBs and relative fluorescence intensity in each U87 and L02 cell.

demonstrating the specificity and reliability of AuNP-MBs. To exclude the possibility that differences in AuNP-MB uptake affected the fluorescence signal, hyperspectral microscopy was used to image the intracellular AuNP-MBs (Figure 3b), and inductively coupled plasma atomic emission spectroscopy (ICP-AES) was used to quantify the relative amount of AuNP-MBs in each cell (Figure 3c). Both U87 and L02 cells showed similar uptake of AuNP-MBs after incubation for 1.5 hours. Consequently, the fluorescence intensity was associated with telomerase activity rather than the total amount of AuNP-MBs inside the cells. Therefore, the AuNP-MBs provide a promising strategy for monitoring intracellular telomerase activity and distinguishing cancer cells from normal cells.

We further designed a telomerase-triggered drug release system by intercalating Dox into the GC base pairs of the hairpin structure of the AuNP-MBs. Because the fluorescence of Dox could be quenched after intercalation,[8] it was calculated that approximately 156 Dox molecules were loaded in one AuNP-MB, named Dox-AuNP-MB. To optimize the sequence length for intercalating more Dox into the beacons, further elongated sequences with 2, 3, 4 and 5 telomeric repeats (Sequence 2, 3, 4 and 5) were designed. The Gibbs free energy of the hybridization was calculated before and after TP extension for each of the designed sequences (Table S1). The calculated energy value difference before and after primer elongation was most obvious in Sequences 2 and 3. From a thermodynamic perspective, Sequences 2 and 3 have a more stable DNA double-strand after primer elongation, implying more efficient substitution of the FITC-labeled 5′ region. Subsequently, laser confocal microscopy was performed to confirm the calculations (Figure S6). The microscopy results demonstrated that Sequences 2 and 3 had both superior detection signals and drug release efficiencies. Thus, Sequence 2 was used in this study for telomerase-triggered sequence substitution and subsequent drug release. The Dox loading efficiency was quantified as 306 Dox molecules per AuNP-MB, named Dox*2-AuNP-MB. After incubation with telomerase and dNTP, nearly 2-times the amount of Dox was released from Dox*2-AuNP-MBs compared to Dox-AuNP-MBs (Figure S7).

We further observed the process of intracellular release of Dox in cancer cells (Figure S8). In the first 2 hours, the Dox fluorescence was observed in the cytoplasm and co-localized with FITC signal, verifying that intracellular Dox release from Dox-AuNP-MBs was triggered by telomerase. With the increase of incubation time, FITC signal still remained in the cytoplasm, but the released Dox was gradually directed to the nucleus for the anticancer function, implying that the AuNP-MB was an efficient Dox loading and delivery system. Three-dimensional confocal imaging further identified the localization of telomerase-triggered FITC fluorescence in the cytoplasm and Dox in the nucleus.

To confirm that the extent of Dox release was dependent on telomerase activity, Dox-AuNP-MBs were incubated with the EGCG-treated U87 cells to visualize the release of Dox. The fluorescence intensity of FITC and Dox gradually reduced with increasing amounts of EGCG (Figure S9), indicating that Dox-AuNP-MBs could be used not only for monitoring telomerase activity but also for the controlled release of Dox in response to varying levels of telomerase activity.

Meanwhile, different cell lines with varying telomerase expression, including U87, MCF-7, L02, and HEK293, were treated with Dox-AuNP-MBs and the fluorescence signals were compared (Figure S10). More abundant fluorescence was observed in U87 cells than MCF-7 cells, while the noncancerous L02 and HEK293 cells showed almost no visible Dox signal. The observed fluorescence was consistent with the telomerase expression in these cells (Figure S5b), confirming the selective drug release of Dox-AuNP-MBs in cancer cells.

To simulate the complex in vivo microenvironment that commonly occurs, in which cancer cells reside amongst noncancerous cells, U87 (cancer cells) and L02 (normal cells) were co-cultured to evaluate the cancer-cell-specific drug release of Dox-AuNP-MBs. For comparison, free Dox, without intercalation into the hairpin DNA sequence, was physically mixed with AuNP-MBs as a control for parallel experiment. As shown in Figure 4, in the control group, the FITC signal was only observed in U87 cells, implying the

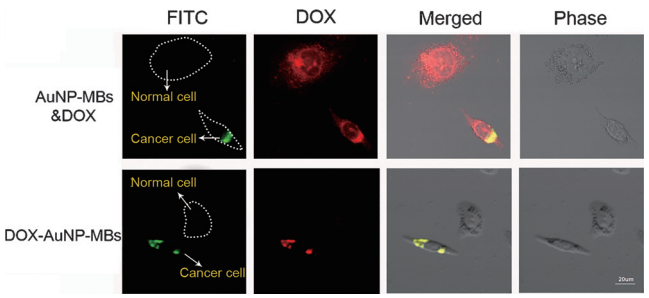

Figure 4. CLSM images of co-cultivation of U87 cells (cancer cells) and L02 cells (normal cells) after incubation with Dox-AuNP-MBs and the mixture of AuNP-MBs and free Dox. Red: Dox; green: FITC; yellow: co-localization of red and green pixels. Scale bar = 20 μm.

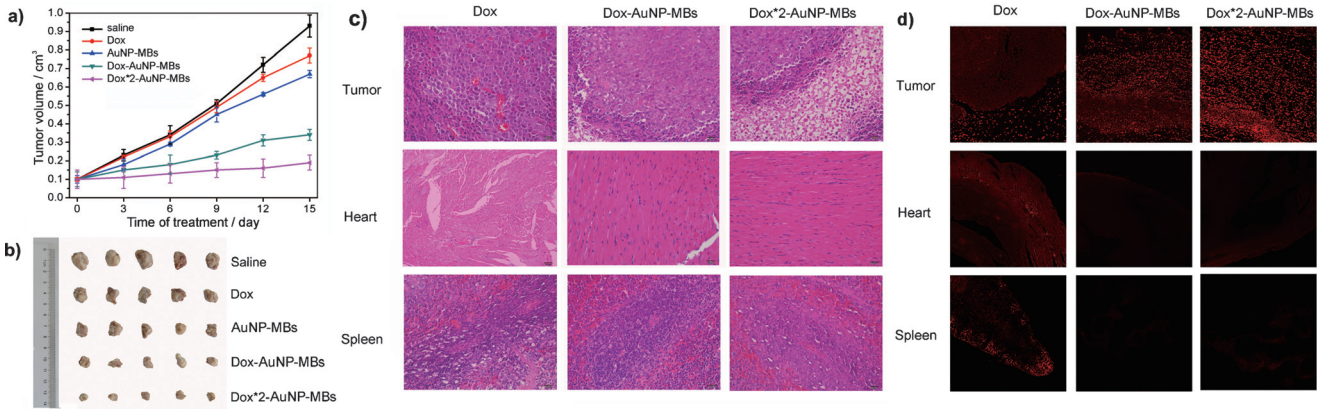

Figure 5. a) Tumor growth curves of the U87-tumor-bearing mice after intravenous injection with saline, Dox, AuNP-MBs, Dox-AuNP-MBs, or Dox*2-AuNP-MBs. b) Images of the tumors collected from the mice at Day 15. c) H&E stained images of tumor, heart, and spleen sections collected from different Dox treatment groups. d) CLSM images of the tissue samples of tumor, heart, and spleen from different treatment groups.

selective telomerase response in cancer cells. However, the Dox fluorescence was found in both U87 and L02 cells, indicating the non-selectivity of Dox itself and toxicity to normal cells. In contrast, for the Dox-AuNP-MB-treated group, both FITC and Dox signals were only shown in U87 cells, suggesting the reliability of telomerase detection and specificity of Dox release in cancer cells.

To examine the in vitro tumor inhibition efficacy and side effects of the telomerase-triggered Dox-delivery system, the MTT assay was performed on L02 and U87 cells (Figure S11 a). No significant loss of viability was found in L02 cells in MB-treated groups, compared to the free Dox group. However, in U87 cells, a significant decrease in cell survival was observed after Dox-loaded AuNP-MB treatment, owing to telomerase-specific release of Dox in cancer cells. The inhibition ratios of Dox*2-AuNP-MBs were higher than Dox-AuNP-MBs, as a result of enhanced Dox release. The cell apoptosis data obtained by flow cytometry also demonstrated the specific and precise cancer cell inhibition (Figure S11 b).

Next, the in vivo antitumor efficacy was investigated by using athymic nude mice subcutaneously injected with U87 cells as the animal model. After intravenous injection, both the Dox-AuNP-MB- and Dox*2-AuNP-MB-treated groups showed remarkably higher inhibition of tumor growth compared to the saline-treated control group, which was due to the enhanced permeability and retention effect of the molecular beacon system and the telomerase-triggered Dox release in tumor sites. Notably, Dox*2-AuNP-MBs showed a significant improvement in tumor-size-inhibition compared to that of Dox-AuNP-MBs, which is the result of the increased Dox loading (Figure 5 a,b). In contrast, only a slight reduction in tumor size was found in mice treated with free Dox, which is likely due to insufficient tumor accumulation. No significant change in body weight was found over the course of the treatments (Figure S12).

To identify tumor inhibition and potential side effects, the three Dox-treated mice groups (Dox, Dox-AuNP-MB, and Dox*2-AuNP-MB) were sacrificed for histologic analysis of tumor and major organs (Figure S13). In the Dox-treated group, heart and spleen toxicity was obvious, as indicated by damaged cardiac tissue structures and decreased splenic corpuscle number, whereas tumor tissues showed nearly no apoptosis. For the groups treated with Dox-loaded AuNP-MBs, markedly increased apoptotic and necrotic tumor cells were observed in the tumor region, while no damage was found in the heart and spleen (Figure 5 c). Laser confocal microscopy was used to examine the distribution of Dox (Figure 5 d). The free Dox treatment resulted in a widespread distribution of Dox fluorescence in tumor, heart, and spleen, which could explain the low tumor inhibition and high toxicity to heart and spleen. As anticipated, Dox-loaded AuNP-MBs showed nearly no Dox signal in normal organs, while a prominent fluorescence signal was detected in the tumors. In particular, the Dox*2-AuNP-MB-treated group exhibited significantly higher Dox fluorescence in tumor tissue than that of the Dox-AuNP-MB-treated group. These results confirmed the tumor-specific release of our MB drug delivery system in vivo, which was triggered by telomerase in cancer cells. Moreover, the barely observable Dox signal in normal tissues demonstrated that the Dox loaded AuNP-MBs were non-responsive in normal organs and stable in vivo. Therefore, the prepared Dox-loaded AuNP-MBs could serve as a potent and versatile tool for telomerase-triggered, cancer-cell-specific detection and drug-targeting with significantly reduced toxicity in normal tissues.

In this study, we have successfully prepared a theranostic system based on the design of a telomerase-triggered molecular beacon, which is highly efficient in both cancer imaging and therapy. This technology will not only assist in the identification of cancer cells, its ability to intrinsically treat only cancerous cells will prevent the undesired death of healthy cells that is commonly seen using more conventional forms of chemotherapy. These findings will also help to inspire future designs of drug delivery systems that respond to cancer-specific biomolecules more accurately.

Acknowledgements

We acknowledge financial support from the National Natural Science Foundation of China (NSFC 81220108012, 61335007, 81371684, 81000666, 81171395 and 81328012); the 973 Key Project (2015CB755504); and the Priority Academic Program Development of Jiangsu Higher Education.

Keywords: drug delivery · molecular beacons · nanoparticles · telomerase · theranostics

How to cite: *Angew. Chem. Int. Ed.* **2016**, *55*, 3304–3308
Angew. Chem. **2016**, *128*, 3365–3369

[1] T. Cech, *Angew. Chem. Int. Ed.* **2000**, *39*, 34–43; *Angew. Chem.* **2000**, *112*, 34–44.

[2] a) H. Q. Yu, D. H. Zhang, X. B. Gu, D. Miyoshi, N. Sugimoto, *Angew. Chem. Int. Ed.* **2008**, *47*, 9034–9038; *Angew. Chem.* **2008**, *120*, 9174–9178; b) M. Hengesbach, N. K. Kim, J. Feigon, M. D. Stone, *Angew. Chem. Int. Ed.* **2012**, *51*, 5876–5879; *Angew. Chem.* **2012**, *124*, 5978–5981.

[3] a) Z. Xiao, C. Ji, J. Shi, E. M. Pridgen, J. Frieder, J. Wu, O. C. Farokhzad, *Angew. Chem. Int. Ed.* **2012**, *51*, 11853–11857; *Angew. Chem.* **2012**, *124*, 12023–12027; b) T. T. T. N′Guyen, H. T. T. Duong, J. Basuki, V. Montembault, S. Pascual, C. Guibert, J. Fresnais, C. Boyer, M. R. Whittaker, T. P. Davis, et al., *Angew. Chem. Int. Ed.* **2013**, *52*, 14152–14156; *Angew. Chem.* **2013**, *125*, 14402–14406; c) J. Tian, L. Ding, H. Ju, Y. Yang, X. Li, Z. Shen, Z. Zhu, J.-S. Yu, C. J. Yang, *Angew. Chem. Int. Ed.* **2014**, *53*, 9544–9549; *Angew. Chem.* **2014**, *126*, 9698–9703; d) S. Hernot, A. L. Klibanov, *Adv. Drug Delivery Rev.* **2008**, *60*, 1153–1166; e) S. A. Stanley, J. E. Gagner, S. Damanpour, M. Yoshida, J. S. Dordick, J. M. Friedman, *Science* **2012**, *336*, 604–608.

[4] D. Hanahan, R. A. Weinberg, *Cell* **2011**, *144*, 646–674.

[5] a) H. Pei, L. Liang, G. Yao, J. Li, Q. Huang, C. Fan, *Angew. Chem. Int. Ed.* **2012**, *51*, 9020–9024; *Angew. Chem.* **2012**, *124*, 9154–9158; b) L. Liang, J. Li, Q. Li, Q. Huang, J. Shi, H. Yan, C. Fan, *Angew. Chem. Int. Ed.* **2014**, *53*, 7745–7750; *Angew. Chem.* **2014**, *126*, 7879–7884.

[6] a) Q. Cheng, Y. Huang, H. Zheng, T. Wei, S. Zheng, S. Huo, X. Wang, Q. Du, X. Zhang, H. Y. Zhang, et al., *Biomaterials* **2013**, *34*, 3120–3131; b) L. Jabr-Milane, L. V. Vlerken, H. Devalapally, D. Shenoy, S. Komareddy, M. Bhavsar, M. Amiji, *J. Controlled Release* **2008**, *130*, 121–128; c) W. Wang, Q. Q. Wei, J. Wang, B. C. Wang, S. H. Zhang, Z. Yuan, *J. Colloid Interface Sci.* **2013**, *404*, 223–229.

[7] a) S. A. Jensen, E. S. Day, C. H. Ko, L. A. Hurley, P. Janina, F. M. Kouri, T. J. Merkel, A. J. Luthi, P. C. Patel, J. I. Cutler, et al., *Sci. Transl. Med.* **2014**, *5*, 209ra152; b) J. Conde, F. Tian, Y. Hernández, C. Bao, D. Cui, K. P. Janssen, M. R. Ibarra, P. V. Baptista, T. Stoeger, J. M. de la Fuente, *Biomaterials* **2013**, *34*, 7744–7753.

[8] G. Qiao, L. Zhuo, Y. Gao, L. Yu, N. Li, B. Tang, *Chem. Commun.* **2011**, *47*, 7458–7460.

Received: September 30, 2015
Revised: December 23, 2015
Published online: February 5, 2016

